

Université de Nantes  
U.F.R Sciences et Techniques  
2017-2018  
Pr. Fritsch  
Dr. Rondeau

Diplôme d'Université de Gemmologie

# EXPERIMENTAL DISSERTATION

## ETHIOPIAN EMERALDS

Brian Carr Smith

## TABLE OF CONTENTS

### Introduction

1. Discovery of Ethiopian Emerald
2. Mine to Market
3. Sampling
  - 3.1 Sample collection methodology
  - 3.2 Samples and sources chart
4. Geology of Emerald
  - 4.1 Geology of East Africa
  - 4.2 Geology of Seba Boru District
5. Experimental Methods
  - 5.1 Basic instruments
  - 5.2 Microscopy
  - 5.3 Spectroscopy
    - 5.3.1 UV – Vis – NIR
    - 5.3.2 MicroRaman
    - 5.3.3 Raman and FTIR
    - 5.3.4 SEM EDS
6. Results
  - 6.1 Classical gemology
    - 6.1.1 Test summary
  - 6.2 Microscope observation
  - 6.3 Spectroscopy
    - 6.3.1 UV – Vis – NIR
    - 6.3.2 FTIR
    - 6.3.3 MicroRaman
    - 6.3.4 SEM EDS inclusion analysis
7. Discussion
- Conclusion
- Acknowledgements
- References



## INTRODUCTION

Of the Big Three colored stones, emerald seems to receive the least attention in the Western World. Perhaps this is due to the fact that the gems that are the most prized are those that are loupe-clean; but emeralds are usually included and most fine emeralds are still assumed to have oil filling of fractures. The fact that the finest no-treatment top emeralds are always priced above top sapphires and competitive with colorless carat diamonds (Appendix 1) points to the fact that this gem is one of the rarest, and hints at a perhaps unfamiliar source of demand.

For centuries the Ottomans, Persians and Mughals were the main market for the emeralds mined by the Spanish after their conquest of Colombia. A visit to Topkapi Palace in Istanbul or the Central Bank of Iran in Tehran reveals the fascination with emeralds in the Near East (Figure 1). Green is the color of Islam: like an oasis in the desert, green is the color of life itself.



Figure 1. A large Colombian emerald crystal in gilded cage, commissioned by Sultan Ahmet I in 1617, was hung above the sultan's throne as a part of the regalia ([bloganavazquez.com](http://bloganavazquez.com)). The Emerald Dagger commissioned by Ottoman Padishah Mahmud the First as a gift for Nadir Shah of Persia ([boutiqueottoman.com](http://boutiqueottoman.com)).

## 1. DISCOVERY OF ETHIOPIAN EMERALD

Only 20 regions around the world have ever produced emerald. The oldest was in ancient Egypt. New discoveries of emerald mines are exceedingly rare, especially when compared to the seemingly regular discoveries of new sources of ruby and sapphire. This decade, however, a new deposit of emerald was discovered in Ethiopia, the first new country of origin since China at Davdar in 2005 (Saeseaw et. al, G&G 2014). Although some artisanal miners may have been finding emeralds in Southern Ethiopia as early as 2004 ([blueniletrade.com](http://blueniletrade.com)), beginning in 2010 reports from Farook Hashami of aquamarines and emeralds brought widespread attention to the possibility of a new gem find in Ethiopia (G&G, Spring 2012). Even so, only five gemological articles about the discovery have been published to date: two by GIA (2012, 2017), one by ICA (2017), one by SSEF (2018), and one by Gem Guide (2018).

In 2015 Gemfields started exploring for emeralds at a concession near Web, Ethiopia (G&G, Spring 2017) but the big find came when two miners near Shakiso, while panning for tantalum, discovered emerald (Figure 2) (InColor, 2017).

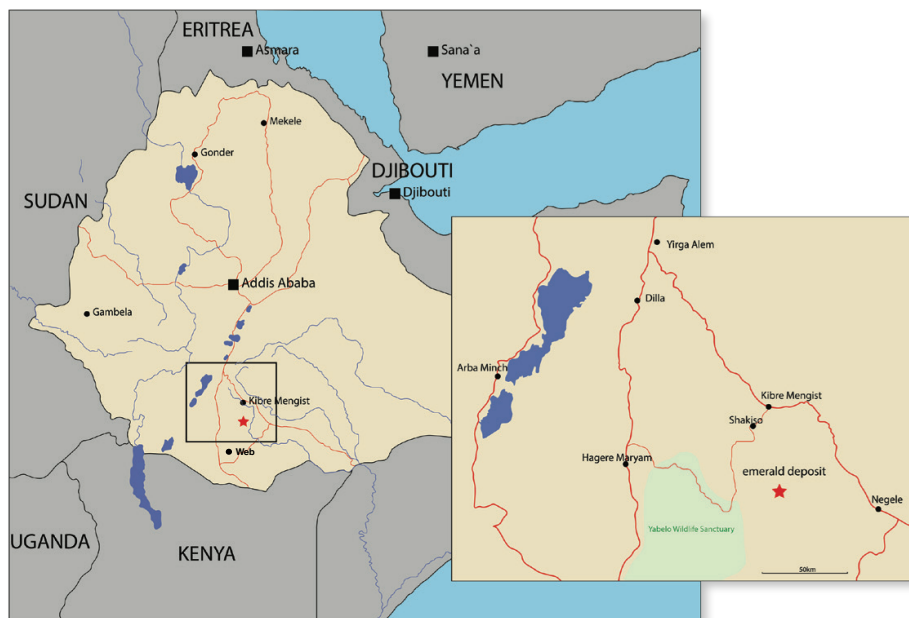


Figure 2. Shakiso is located about 10 hour drive from Addis Ababa and the mining area of Haloo, Seba Boru is about two hours further south (InColor, 2017).

## 2. MINE TO MARKET

The first low grade emerald crystals started appearing in 2016 in Tuscon and did not cause a stir. A year later in 2017, fine-quality cut gems arrived and Tuscon was abuzz with excitement. During the ICA conference in Jaipur in October, 2017, tables-full of rough were seen on the desks of big emerald cutters (Figure 3).



Figure 3 (two photos). Russian gem dealer Alexey Burlakov inspects a large parcel of strongly saturated Ethiopian emerald rough in Jaipur, October 2017. (Photos: Brian Smith)

By Spring of 2018 Ethiopian emeralds were widely available in Tuscon. It has been estimated that up to 20 Kg of mixed grade material per month is now being produced in the area Southern Ethiopia ([blueniletrade.com](http://blueniletrade.com)). GIA estimated that 100 Kg had been produced by early 2017 (G&G, Spring 2017). When low, medium and high grade material is considered, up to three tons may have been produced by April 2017 (InColor, Spring 2017).

What is remarkable about Ethiopian emeralds is that the top grade material is often free of fractures and hence also oiling. Much like the Russian Malysheva emerald, or a percentage of Zambian material, the top grade Ethiopian emerald is being sold as a “no treatment” stone. This places Ethiopia on the top shelf of emerald origins; where beauty, and price, reach the sky.

### 3. SAMPLING

11 samples were analyzed for this report from three sources.

#### 3.1. Sample Collection Methodology

Although I recall hearing about Ethiopian emeralds at Tuscon in early 2017 I do not recall seeing any. When I traveled to Jaipur in October, 2017 I saw large volumes of Ethiopian rough for the first time, but dealers were unwilling to part with even chips for my analysis.

Upon arrival in Nantes in November 2017 I discovered that Dr. Rondeau had already received emerald samples through his channels in Ethiopia (Rondeau has done research on Ethiopian opal) and had already sliced and mounted the samples on a slide for analysis. These samples of Ethiopian origin and will be referred to as BR 4-7.

In communications with UK gemologist Rosie Perkins, who is working on a project at Lotus Gemology in Bangkok, I discovered that Bangkok-based US gem dealer Jeffrey Bergman had acquired Ethiopian rough and was cutting emeralds for sale in Tuscon. The offcuts were available for analysis and could be shipped to me in Nantes. These samples arrived by FedEx in time for the last week of class in early December. Only one offcut was suitable for study. This sample will be referred to as JB 12.

Finally, at Tuscon in 2018 an Ethiopian woman approached me at Zoe Michelou's booth where Jean Claude Michelou's Swat, Pakistan emeralds were on display in the vitrines. She asked if I bought emerald and I enthusiastically replied, "Yes!!!" Her name is Sablework Abay and she stated that she is from Shakiso and that her husband's family owns the hill at Haloo, Seba Boru on which the emeralds are being mined (Figure 4). She pulled large plastic bags of low to medium grade rough out of her backpack, which we spread onto paper plates for sorting and I purchased a selection of the best crystalized samples. These samples will be referred to as SW1-6 (Figure 5).





Figure 4. Mining community near Haloo, Seba Boru ([blueniletrade.com](http://blueniletrade.com))



Figure 5. Sablework Abay from Shakiso, Ethiopia displays her rough emeralds for sale. This grade was available in Tuscon February, 2018 for \$30/gram.

### 3.2 Samples and Sources Chart

These are the samples that were collected and analyzed (Figure 6).

Sample	Photo	Color	Length	Width	Depth	Weight	Comments
<b>BR 4</b>		Slightly bG	3mm	4mm	Approx 1mm	Approx 0.20 ct	Glued to slide
<b>BR 5</b>		Slightly bG	4mm	5mm	Approx 1mm	Approx 0.30 ct	Glued to slide
<b>BR 6</b>		Slightly bG	7mm	5mm	Approx 1mm	Approx 0.50 ct	Glued to slide
<b>BR 7</b>		Saturated G	5mm	5mm	Approx 1mm	Approx 0.40 ct	Glued to slide
<b>JB 12</b>		Light bG	12mm	7mm	2.5mm	1.35 ct	Hexagonal offcut
<b>SW 1</b>		Dark G	6mm	4.5mm	4mm	0.89 ct	Flat tabular prism
<b>SW 2</b>		V light bG	5.5mm	5.5mm	3mm	1.57 ct	Flat tabular prism
<b>SW 3</b>		Light bG	10mm	6mm	6mm	4.03 ct	Prism w/ matrix
<b>SW 4</b>		Light bG	8mm	8mm	8mm	4.17 ct	Prism w/ matrix
<b>SW 5</b>		bG	14mm	7.5mm	6mm	5.24 ct	Prism w/ matrix
<b>SW 6</b>		Light bG	10mm	6mm	6mm	2.93 ct	Prism w/ matrix

Figure 6. Samples from Benjamin Rondeau (BR 4-7, not prepared with regard for crystallographic orientation), Jeffrey Bergman (JB 12), and Sablework Abay (SW 1-6).

#### 4. GEOLOGY OF EMERALD

The rarity of emerald in the mineral composition of the earth is due to the unusual combination of geological events required for emerald to form. Emerald deposits are much more rare than ruby or diamond, less than 50 worldwide, because elements from the oceanic crust must come in contact with rare elements from the continental crust before formation can occur (Rondeau, Class Notes, 2017).

Emerald belongs to the beryl family, an uncommon mineral in the continental crust. In order for beryls to form the rare element beryllium, from granite/pegmatite intrusions of the continental crust, plus aluminum, silicon and oxygen, must be dissolved in a heated mineral-rich solution and allowed to cool. In addition, for these beryls to be of the emerald variety, this solution must contain chromium and/or vanadium. These are the chromophores which create the green in beryl, and which are typical of the oceanic crust. Chromium and vanadium are trapped by organic matter in the ocean, the remains of which subsequently form oceanic sedimentary rocks. These rocks are later subducted and metamorphosed into basic rocks in the earth's upper mantle. Through magmatic or tectonic activity, when these metamorphic basic Cr/V-bearing rocks come in contact with Be-rich pegmatites in the continental crust, there is a possibility of emerald formation (Schwarz and Pardieu, 2009).

But not all emeralds form under the same conditions. In fact there may be as many different genetic origins for emerald as there are similar. To quote Schwarz and Pardieu, "The geological background situation explains why certain gemological features can be very similar in emeralds from different deposits, but also why others may have a locality-specific character. There is a close relationship between the genetic environment (especially nature and mineralogical composition of the host rock) and the mineralogical-gemological properties of emeralds." (Schwarz and Pardieu, 2009)

#### 4.1. Geology of East Africa

Ethiopia lies at the northern end of the Mozambique Metamorphic Belt (MMB), which extends from the Red Sea to Mozambique. Between 500 and 650 million years ago the formation of Gondwanaland along this suture was the source of major mountain building and metamorphic events. During this process subducted ocean crust was folded, faulted and metamorphosed into rocks like schists along the suture. These rocks also moved closer to the surface of the continental crust.

#### 4.2. Geology of Seba Boru District

In the Seba Boru District along the same MMB suture, at some later point in time, granitic-vulcanism-related pegmatites encountered those chromium-rich mica schists. These pegmatites are known for their rare-elements and are the source of the largest tantalum reserves in Ethiopia. Tantalum-rich pegmatites are also known for their high concentrations of beryllium (InColor, 2017). In the contact zone between these pegmatites and schists, emerald mineralization occurred through metasomatism. (Gem Guide, 2018).

### 5. EXPERIMENTAL METHODS

To perform gemological tests on the emeralds a variety of diagnostic and measurement tools were used, starting from the most basic and progressing to the most advanced.

#### 5.1 Basic Instruments

Initial observation of gemstones includes use of measure of size, weight, color, and any special features. Then we progress to the basic handheld tools of gemology: 10x loupe, London dichroscope, hand-held diffraction grating spectroscope and Chelsea color filter. Finally we use desktop tools: refractometer, polariscope and ultra-violet cabinet (long wave ultra-violet – LWUV – at 365 nm, and short wave ultra-violet – SWUV – at 254 nm).



## 5.2. Microscopy

I used a 70x Leica Microscope with attached camera and Leica desktop photo software to observe and create photomicrographs of inclusions.

## 5.3 Spectroscopy

Spectroscopy for this study used UV-Vis-NIR (ultraviolet – visible – near infrared), MicroRaman and SEM EDS spectrometers.

### 5.3.1 UV-Vis-NIR

UV-Vis-NIR spectroscopy is the primary method used to determine the origin of color in the emeralds. The spectra were recorded in absorbance on a Perkin Elmer Lambda 1050. Spectral resolution is 1 nm from 325 to 1,800 nm and 2 nm from 1800 to 2500 nm. Photomultiplier tubes (PMT) detector is set with a data interval of 1 nm (response 0.20 s) from 325 to 860 nm. Indium-gallium-arsenide (InGaAs) detector is set with a data interval of 1 nm (response 0.2 s) from 860 to 1,800 nm. PbS Amplified (PbS) detector is set with a data interval 2 nm and a detector setting of 1.0. Spectra were later manually set in Apple Numbers in absorption coefficient to allow comparison between samples.

### 5.3.2 Raman and FTIR

Vibrational spectroscopy tools were tested on samples but without a specific methodology or understanding of how results could be useful. It was later thought that since the focus of this dissertation is the gemological features of natural emerald crystals from a specific locality, that the typical synthetic and treatment identification placed vibrational spectroscopy out of scope. Unfortunately, it was discovered close to the submission deadline that water orientation within vacancies in emerald unit cell channels may constitute a key test in determining genetic origin. One FTIR result for ordinary ray spectrum of JB12 has been included but *all samples should be tested* to learn if all are Type 2 emeralds. The spectrometer was a Bruker Alpha Fourier Transform Infrared spectrometer with a spectral range of 2000-7000  $\text{cm}^{-1}$  and a spectral resolution of 2  $\text{cm}^{-1}$ .

### 5.3.3 MicroRaman

MicroRaman is used for analysis inside stones to identify inclusions of particular interest. Samples, first analyzed for inclusions under the microscope in immersion liquid, were subsequently polished to reveal inclusions in greater clarity for analysis with MicroRaman. Of the two machines available at Univ. de Nantes we found the Geology Department's LabRaman LABSP4.18-06 to be much more user friendly. Detector was set to CCD1 with a power of 50MW for 30 seconds. Inclusions were pinpointed at 50x for spectroscopic analysis. We did not like the horrible Horiba microRaman at IMN and thought the brand name was certainly a joke. Raman spectra were later evaluated via Crystal Sleuth, and in reference to additional cited literature, to determine the nature of inclusions.

### 5.3.4 SEM Chemical Analysis

The scanning electron microscope (SEM) used is a JEOL JSM-5800. SEMs can only view and analyze the surface of samples. Images can also be captured up to 1,000,000x magnification on some SEMs. BR4-7 (on the slide) were coated with amorphous carbon and then surveyed for interesting surface reaching inclusions. Chemical analysis of inclusions was also tested using energy dispersive x-ray spectroscopy (EDS). The EDS detector analyses the relative concentrations of elements at the surface of samples. When these concentrations are normalized for the atomic weight of elements identified, we can chemically identify the molecular makeup of surface crystal matrix and surface reaching inclusions. The EDS function of SEM is not a suitable technique for the analysis of minor and trace elements (Wainer, 2017) so we did not attempt these tests.

## 6. RESULTS

Classical gemology revealed several interesting characteristics of these Ethiopian emeralds. Microscopy proved surprising in terms of the variety, nature and complexity of inclusions discovered. UV-VIS-NIR absorption spectrums proved the origin of color. MicroRaman identified components of complex inclusions inside the crystal and SEM EDS chemically identified others at the surface.

### 6.1 Classical Gemology

Classical gemology mostly delivered the expected results although there were several items of note. In general observation SW1 and SW2 were interesting for their flat, tabular, crystal habit as very short prisms are not very common for emerald. Next, the RIs tended to be high, similar to other schist-hosted emeralds (Saeseaw et al, 2014), which could be attributed to water in the channels or high iron content, thus slightly raising RIs (both will be reviewed further on in results). Pleochroism was generally strong. Spectrums were as expected but weak, in some cases correlating with saturation of the sample (Figure 7). The Chelsea Filter was tested but gave grey to grayish-pink results for all samples and was considered unhelpful. SW/LW UV were inert due to high iron content, typical of schist-hosted emeralds (Saeseaw et al, 2014).


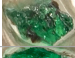

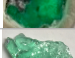







Sample	Photo	Refractive Index	Birefringence	Optic Char.	Crossed Polars	Pleochroism (Dichroscope)	Specific Gravity	Handheld Spectroscope <sup>1</sup>
BR 4 <sup>2</sup>		1.580-1.570	0.010	U -	Blinking	Weak yG, bG	N/A	Violet, 646, 662, 683
BR 5 <sup>2</sup>		1.580-1.570	0.010	U -	Blinking	Weak yG, bG	N/A	Violet, 646, 683
BR 6 <sup>2</sup>		1.585-1.575	0.010	U -	Blinking	yG, bG	N/A	Violet, 646, 662, <u>683</u>
BR 7 <sup>2</sup>		1.587-1.580	0.007	U -	Blinking	yG, bG	N/A	Violet, 646, 662, <u>683</u>
JB 12		1.588-1.580 <sup>3</sup>	0.008	U -	Blink ⊥ C	yG, bG	2.69 g/cm <sup>3</sup>	646, 683
SW 1		1.590-1.580 <sup>4</sup>	0.010	U -	Blink ⊥ C	yG, bG	2.76 g/cm <sup>3</sup>	<u>Violet</u> , <u>646</u> , 662, <u>683</u>
SW 2		1.580 <sup>5</sup>	N/A	N/A	Blink ⊥ C	Strong yG, bG	2.71 g/cm <sup>3</sup>	<u>683</u>
SW 3		1.585-1.578 <sup>3</sup>	0.007	U -	Blink ⊥ C	Strong yG, bG	2.72 g/cm <sup>3</sup>	<u>683</u>
SW 4		1.585-1.578 <sup>3</sup>	0.007	U -	Blink ⊥ C	Strong yG, bG	2.71 g/cm <sup>3</sup>	646
SW 5		1.580 <sup>5</sup>	N/A	N/A	Blink ⊥ C	Strong yG, bG	2.70 g/cm <sup>3</sup>	Violet, 646, 662, <u>683</u>
SW 6		1.590 <sup>5</sup>	N/A	N/A	Blink ⊥ C	Strong yG, bG	2.72 g/cm <sup>3</sup>	Violet, 662, <u>683</u>

Figure 7. 1. Absorption spectrum, strong absorption is underlined. 2. These samples, sliced, polished and glued to a slide, were not prepared with any consideration of crystallographic orientation, although none of them seem to be sliced perfectly perpendicular to the C-Axis based on evaluation of pleochroism with the dichroscope. BR4 and BR5 may have been close to perpendicular as they delivered weak pleochroism. SG could not be obtained due to slide mounting. 3. These crystals were polished on their crystal faces in order to reveal inclusions for photography and MicroRaman identification. After polishing it was possible to document RIs more accurately. 4. This tabular short prism had very flat terminations and it was easily possible to document an RI and optic character. 5. RIs were taken by spot reading.

One source of confusion came up when taking RIs for JB12 and SW3. Both had been polished in a direction perpendicular to the C-axis so inclusions could be analyzed and RIs taken. Strangely both of these samples showed bi-refringence when RIs were measured on facets assumed to have been polished perpendicular to C (ie. either a polished termination or on one end of slice perpendicular to C). Emmanuel explained this could be due to either the angle of polish not being exactly perpendicular to C or that the included nature of these stones was affecting the reading and showing bi-refringence from reflections of angles other than parallel to C.

## 6.2 Microscope Observation

All of the samples studied were moderately included but still had zones of transparency sufficient to allow analysis with multiple gemological tools. Figures 8-15 show some of the common inclusions seen that were not further analyzed.

The first thing I noticed was color concentration. In bright field with immersion, the concentration of chromium towards hexagonal crystal faces and terminations was quite obvious as were center sections of samples, towards the base, that were filled with tube-like channels. This is also typical of Panjshir emeralds from Afghanistan (Saeseaw et al, 2014). Towards the termination all of the the crystals were also significantly less included. Five to 10 percent yields have been reported by cutters and our crystals would also seem to follow those guidelines for zones with good crystal (Figure 8, 9) (Gem Guide, 2018).

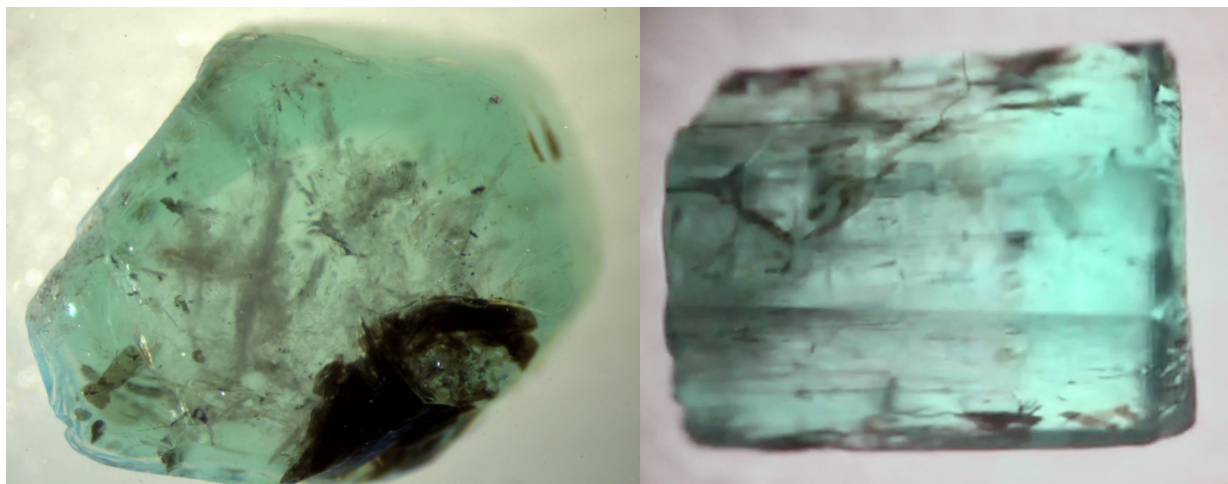


Figure 8 (Left). SW4 in immersion on the left shows color concentration near hexagonal crystal faces. At the right (Figure 9, Right), after faces were polished to reveal inclusions for photomicrography, the better crystal and color concentration towards the termination, and fluid filled channels in the center of the crystal towards the base, are readily apparent @ 10x.

In and around the crystals there is a profusion of irregularly shaped mica. There are also seen pseudo hexagonal platelets seen within the crystal mass (Figure 10).

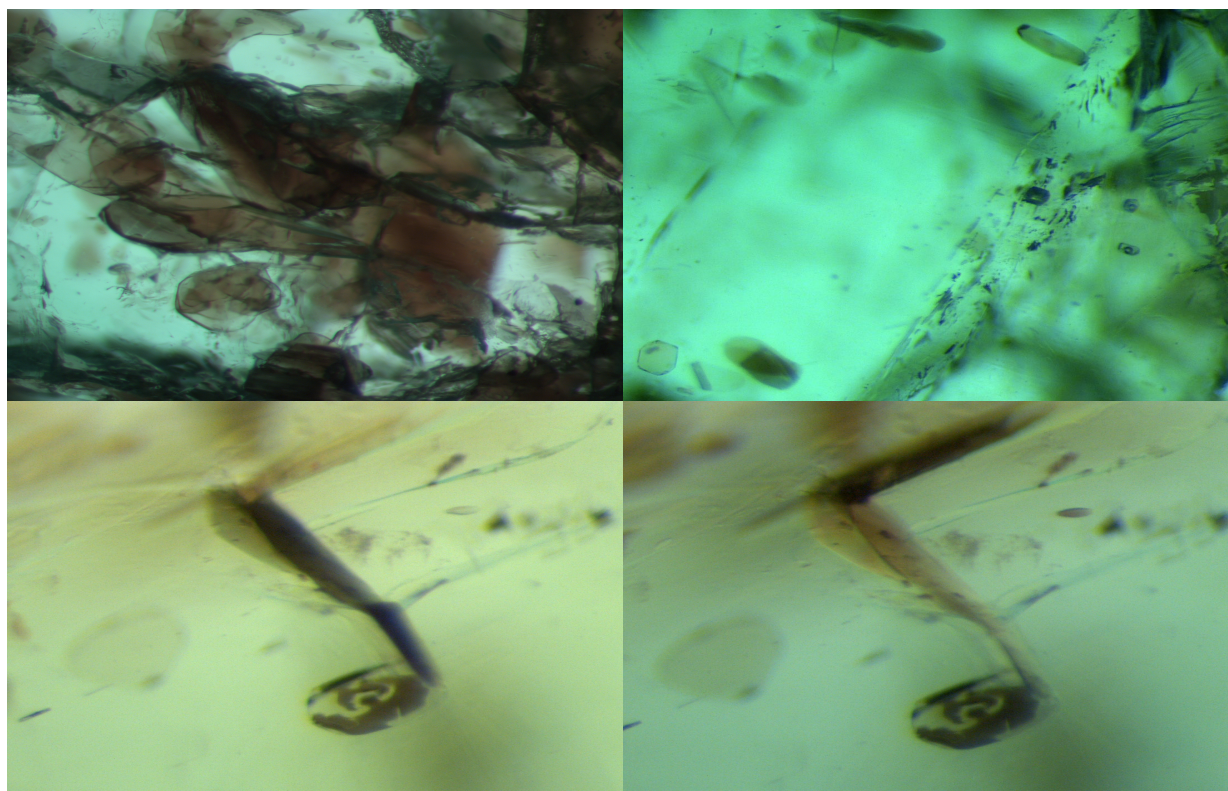


Figure 10 (4 photos). BR5 (Top L) and BR6 (Top R) show micas that are either anhedronal blobs or pseudo-hexagonal platelets @70x. SW3 (Bottom L& R) shows pleochroism of mica viewed in horizontal/vertical polarization @ 70x.



Dark nailhead-type inclusions were seen (Figure 11).

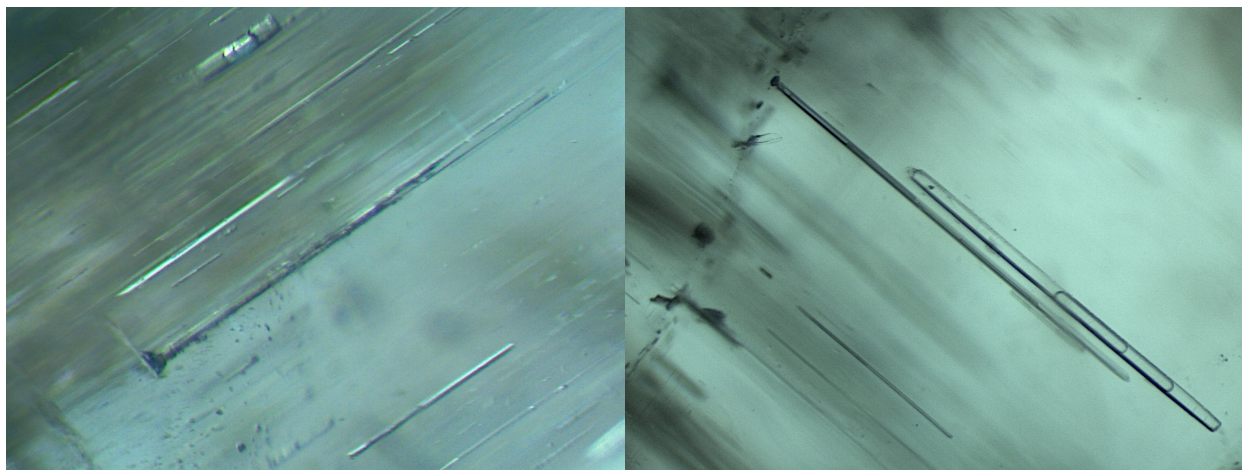


Figure 11 (two photos). SW3 showed several nail-head inclusions @ 70x. The dark material was unable to be identified with Raman microprobe analysis.

Multiphase negative crystal inclusions parallel to the direction of crystal growth, following blockage by a smaller crystal, were frequently seen. Within these cavities multiple immiscible liquids and a gas, sometimes with multiple crystal inclusions, were also seen. Heating the sample can cause one of the liquids to absorb the gaseous phase (InColor, 2017). These inclusions deserve further study to determine if any crystals can be discovered within the gas partition (Figure 12).

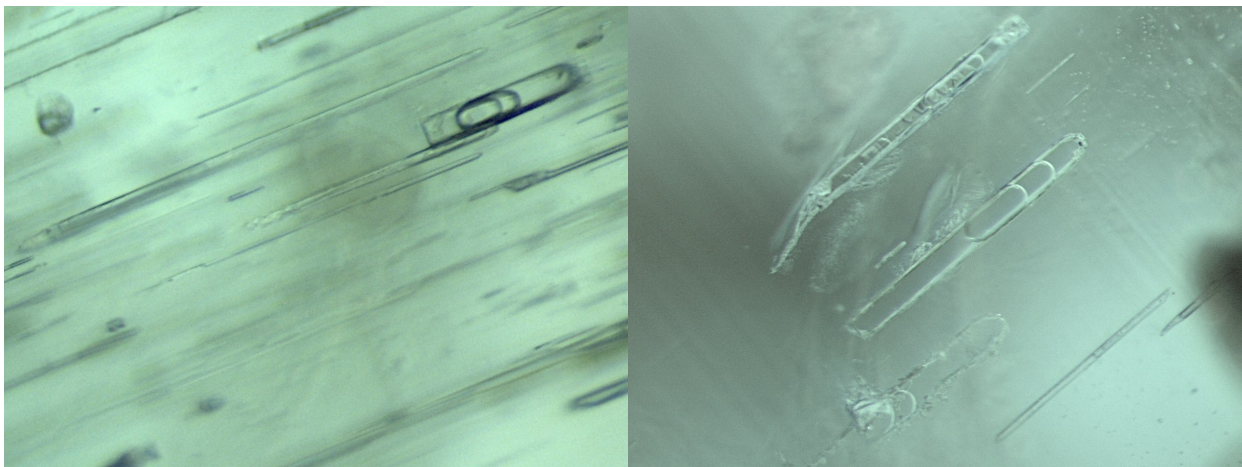


Figure 12 (two photos). SW3 (Left) and SW4 (Right) had many inclusions with two liquid and one gas phase, sometimes with crystals @ 70x.

Fields of blocky two-phase negative crystals parallel to crystal growth, reminiscent of Zambian Kafubu emerald (Saeseaw et al, 2014), veil-like in healed fractures (Figure 13).

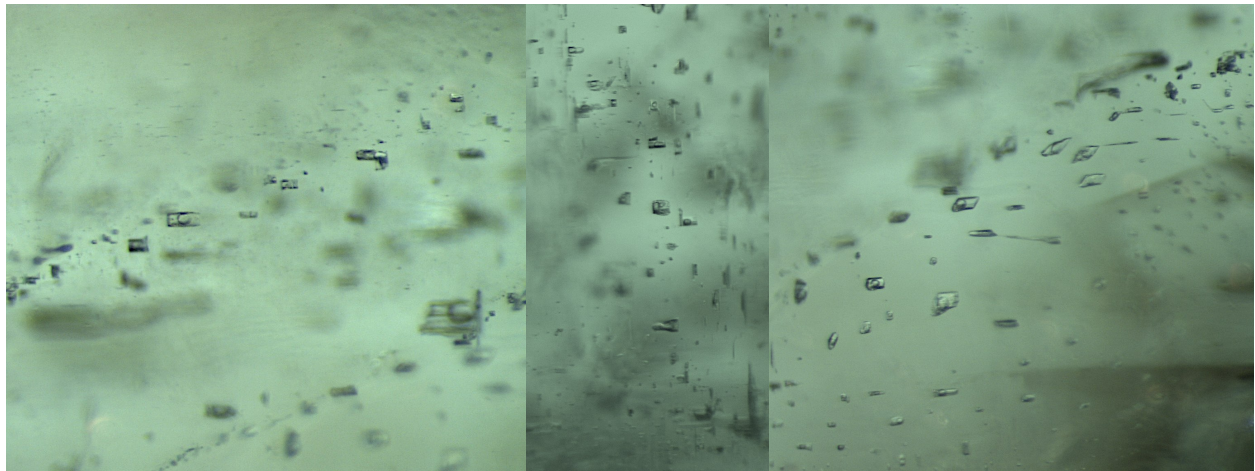


Figure 13 (three photos). SW6 had many two phase inclusions in healed fractures. Seen in immersion @ 70x. Dendritic dark inclusions were less frequent but notably present, also reminiscent of Kafubu (Figure 14) (Saeseaw et al, 2014).

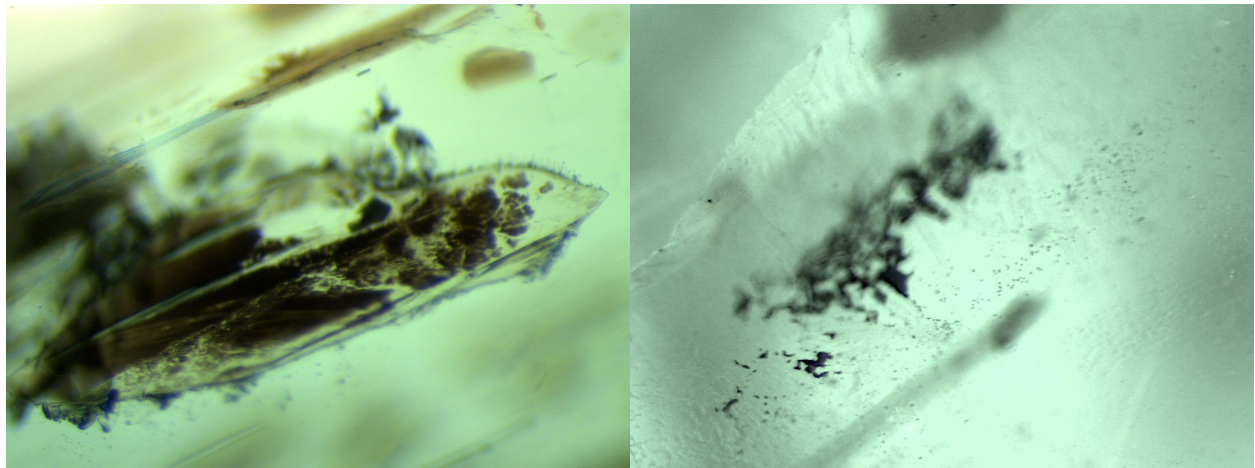


Figure 14. SW3 and SW4 showed dendritic inclusions @ 70x.

The last microscopic observation was of significant interest. In all of the long crystal prisms (SW3-SW6), at the purest crystal “gemmy” end towards the termination, cleavage could be seen. Using a 10x loupe or microscope in transmitted light and tilting slightly away from perpendicular to the C-axis and then back allowed the feature to be seen parallel to the termination. When off perpendicular and then going into perfectly perpendicular to C it was possible to view a Venetian blind-type effect, where color went from green lines parallel to the termination to colorless. It’s amazing to



consider that stacked rows of hexagonal unit cells, when viewed in perfect alignment perpendicular to C, are almost invisible. When viewing the colorless transmitted light coming through the weak bonds in molecular layers, one is actually looking through the gaps in regularly arranged molecules themselves. (Figure 15)

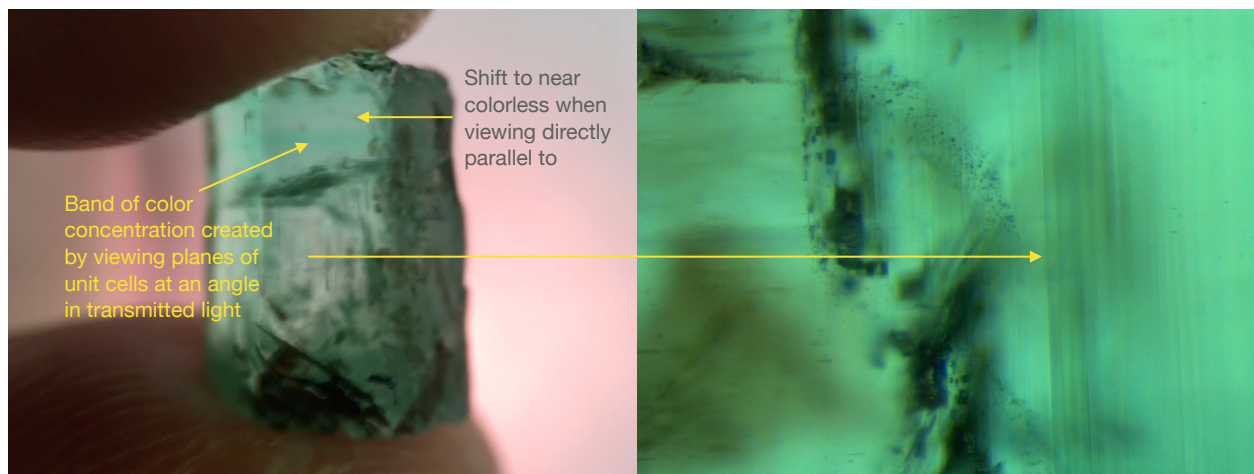


Figure 15 (two photos). SW3 most clearly showed cleavage @ 3x (Left) and 70x (Right, rotated 90 degrees).

## 6.3 SPECTROSCOPY

### 6.3.1 UV – VIS – NIR

UV-VIS-NIR can be helpful in origin determination of emerald but probably more accurately assists in determination of genetic origin. Spectra showed absorptions similar to high-iron schist-based deposits, in particular Kafubu, Zambia. In ordinary ray polarized spectra very strong  $\text{Fe}^{2+}$  absorption was seen as an unusually strong broad band from 700-950nm that was on average 2-3x the amplitude of  $\text{Cr}^{3+}$  at 430 and 601nm. Also like Kafubu and Panjshir, Afghanistan emeralds, a narrow  $\text{Fe}^{3+}$  absorption band at 372nm was observed only in the ordinary ray (Figure 16) (Saeseaw et al, 2014). In extraordinary ray polarized spectra  $\text{Cr}^{3+}$  was seen particularly at 683 and also at 649nm, with some  $\text{Fe}^{2+}$  absorption present but not as strong as chromium (Figure 17). No evidence of  $\text{V}^{3+}$  was seen (like Wood and Nassau, 1968). Peaks between 1000nm and 2500nm correspond to impurity molecules with 1406 and 1893 corresponding to water and  $\text{CO}_2$  (Wood and Nassau, 1968).



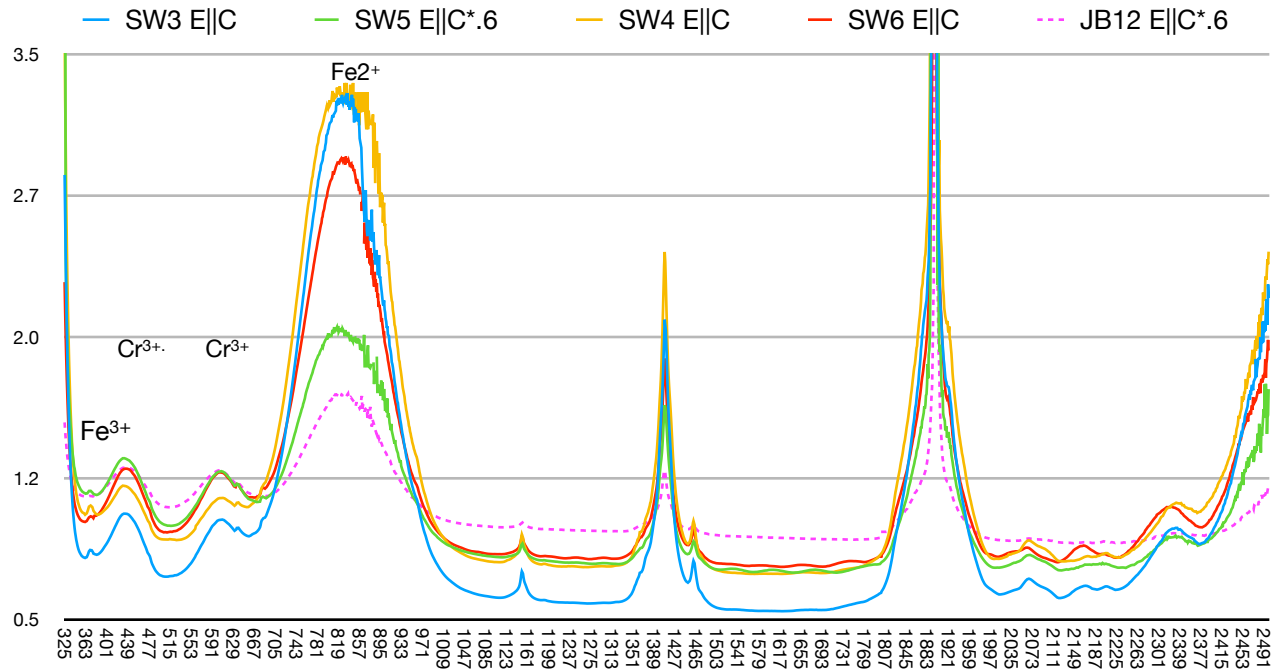


Figure 16. SW3-6 polarized ordinary ray spectra in absorption coefficient. JB12 off-cut's spectrum was not polarized but was captured down the C-axis. Data smoothing was applied, mostly between 850-890nm, to bring S/N back into the range of the curve, where detector change created extreme noise.

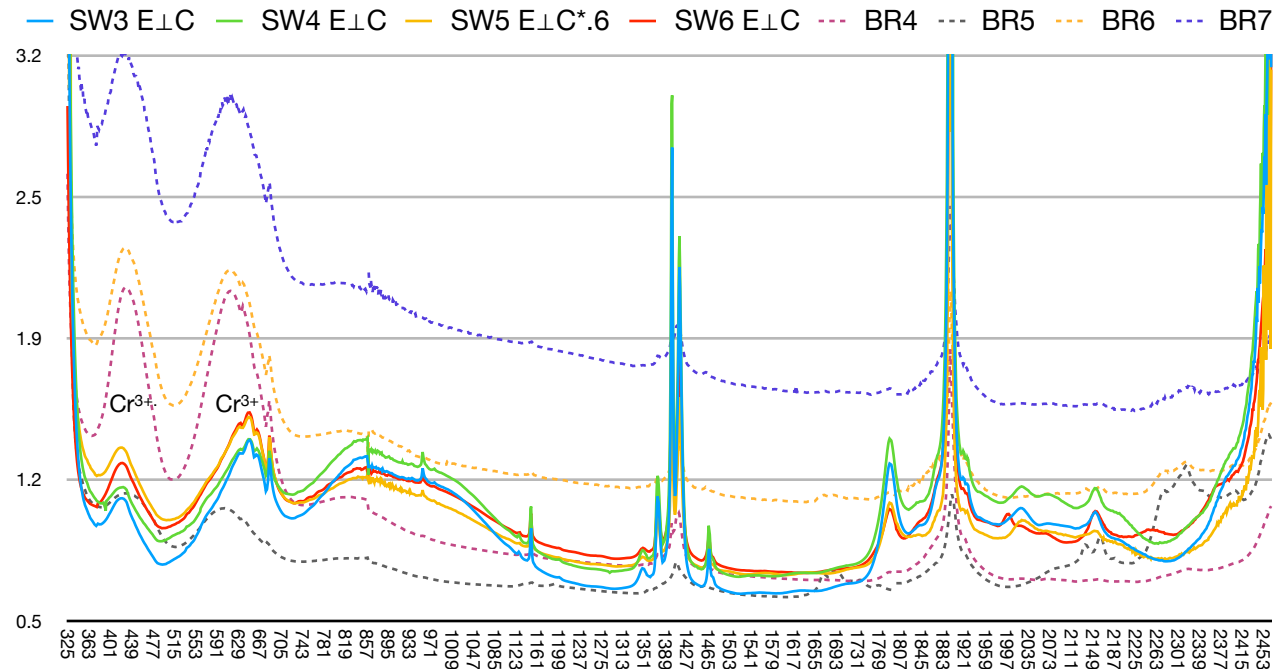


Figure 17. SW3-6 polarized extraordinary ray spectra in absorption coefficient. BR4-7 were captured in the pleochroic direction but not polarized are shown in dotted lines. BR4-7 were slide mounted and close to the same thickness so absorption coefficients were not modified. Minor data smoothing was applied at 860 and 1799nm.

### 6.3.2 FTIR

FTIR results were taken for only one sample and without sufficient range or resolution to be conclusive. Fortunately, although polarization was not used, spectrum was read down the C-axis. The 6842  $\text{cm}^{-1}$  absorption line does hint at a possible Type II orientation of water molecules within silicon channels of emerald unit cells, however, along the C-axis (Figure 18, 19). GIA found that based on a selection of emeralds analyzed in 2014 only Kafubu emeralds were Type II (Figure 220). Also, of interest, GIA's figure caption does not represent their spectrum in the peer-reviewed article. The spectrum is more trustworthy. This FTIR result shows yet another indication that Ethiopian emeralds may be easily confused with Zambian, Kafubu emeralds.

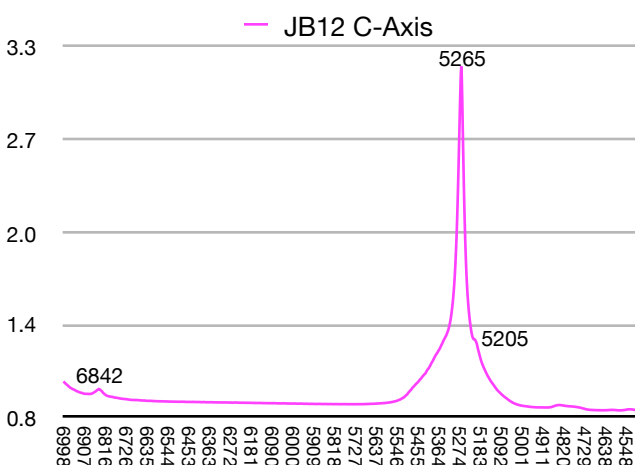


Figure 18. Spectrum shows 6842  $\text{cm}^{-1}$  absorption which appears to indicate this Ethiopian emerald is Type II, making it similar to Kafubu, Zambia emeralds.

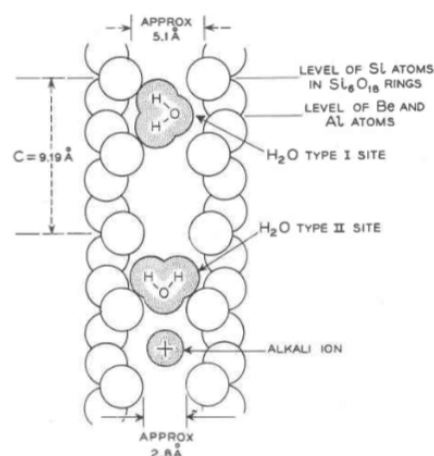


Figure 19. Orientation of water molecules within silicon channels in stacked unit cells (Wood, Nassau, 1968)

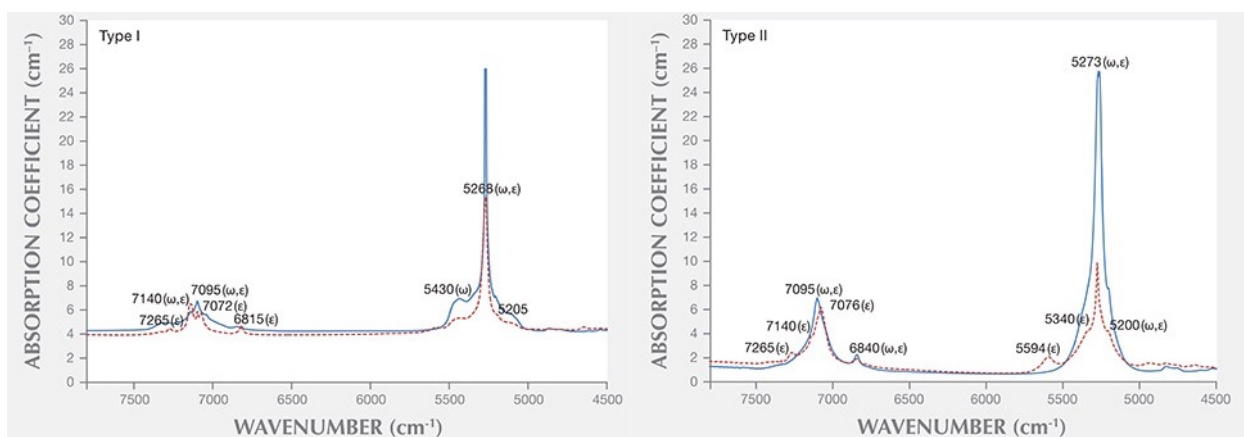


Figure 20. FTIR spectra of a range of emerald samples in 2014, Kafubu, Zambia emeralds at right. Ordinary ray blue, extraordinary ray dotted. (Saeseaw et al, 2014).

### 6.3.3 MicroRaman

We were able to analyze three different samples with MicroRaman: SW3 and SW4, after crystal faces were polished to reveal interesting inclusions previously identified under immersion, and JB12, because it was a very thin and clean sample.

SW3 had interesting multiphase inclusions where a crystal growth had been stopped by a solid creating a nail-head shaped tube that later closed, trapping growth solution. After polishing the crystal face, the inclusion was analyzed by Raman microprobe. Two immiscible liquids, a gas, and a crystal were identified. Liquid 1 was identified as water with peaks at 3596 and 3606  $\text{cm}^{-1}$ . Liquid 2 was identified as  $\text{CO}_2$  liquid with a peaks at 1282  $\text{cm}^{-1}$  and 1386  $\text{cm}^{-1}$ . The gas could be identified as  $\text{CO}_2$  gas that dissolves into the liquid when heated by laser (Figure 21, 22) (Shubnel, 1992). The crystal was identified as a feldspar with a peak at 512  $\text{cm}^{-1}$  (Figure 23) (Pinet, et al, 1992).

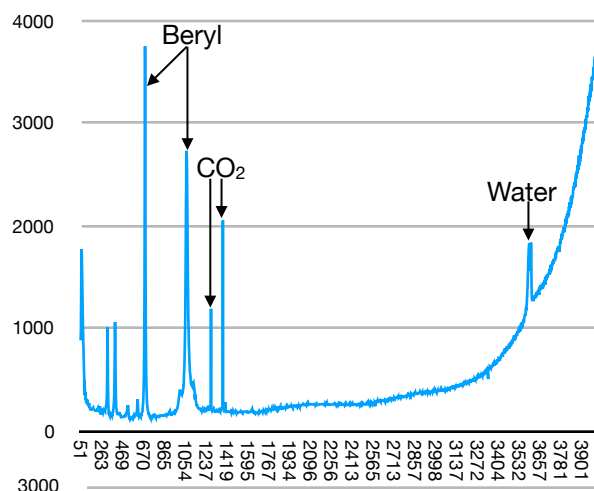
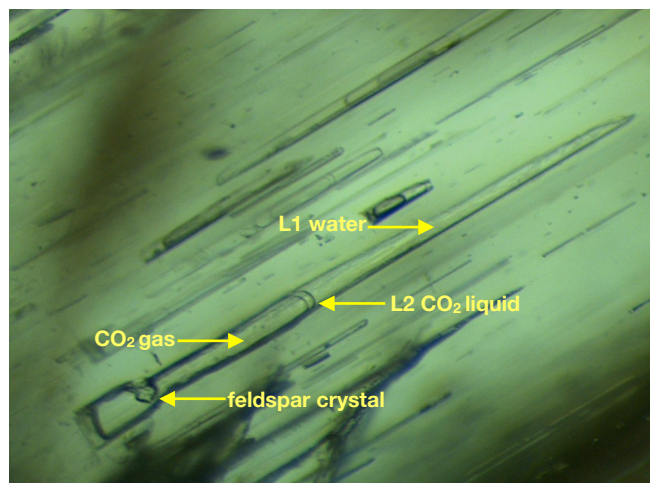
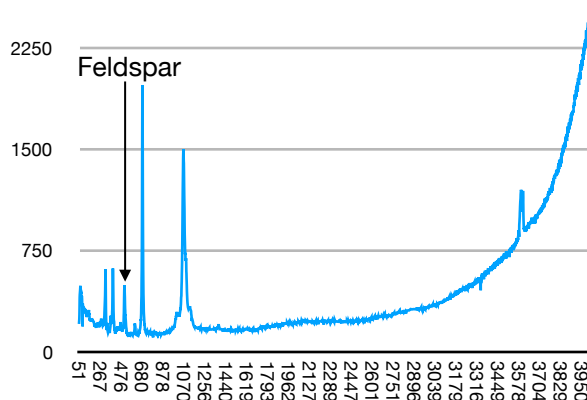


Figure 21 @ 70x (Top Left) shows nailhead inclusion phases. Figure 22 (Top Right) spectrum shows peaks at 687 and 1070  $\text{cm}^{-1}$  for beryl, 1282 and 1386  $\text{cm}^{-1}$  for  $\text{CO}_2$  and 3596 and 3606  $\text{cm}^{-1}$  for water.

Figure 23 (R) shows the spectrum taken for the crystal, which showed a new peak at 512  $\text{cm}^{-1}$ , the main peak for members of the feldspar family.



SW4 had one very interesting multiphase inclusion consisting of a large number and variety of solids, liquids and gasses (Figure 24).

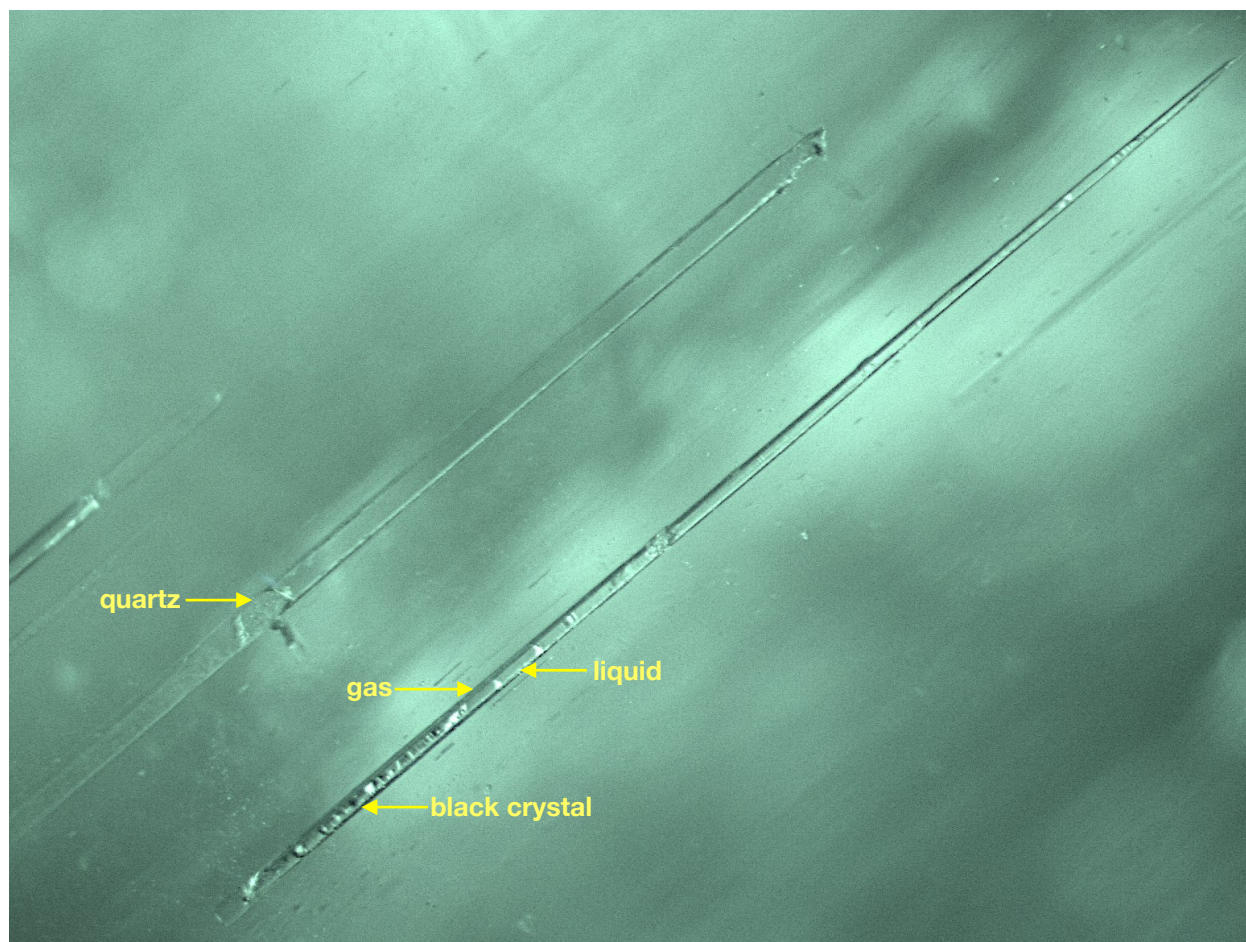


Figure 24 at 70x shows an needle-like negative crystal filled with many solids liquids and gasses. Above it is a negative crystal created by the presence of a crystal with the trigonal habit of quartz.

The black crystal in the multi-phase inclusion was suspected to be a sulfide. The resulting spectrum was obviously a mixture and beryl and quartz spectra were detected (Figure 25). Crystal Sleuth gave a result of Pyrrhotite with peaks at 183, 229, 713, 927, 987, 1097  $\text{cm}^{-1}$  (see Appendix 2). Two principal peaks at 340 and 375  $\text{cm}^{-1}$  could not be identified even though simple gasses were checked. The crystal in the two-phase solid-liquid negative crystal above the multiphase inclusion showed a nice termination and showed a spectrum with peaks at 203 and 461  $\text{cm}^{-1}$  proving quartz (Figure 24).



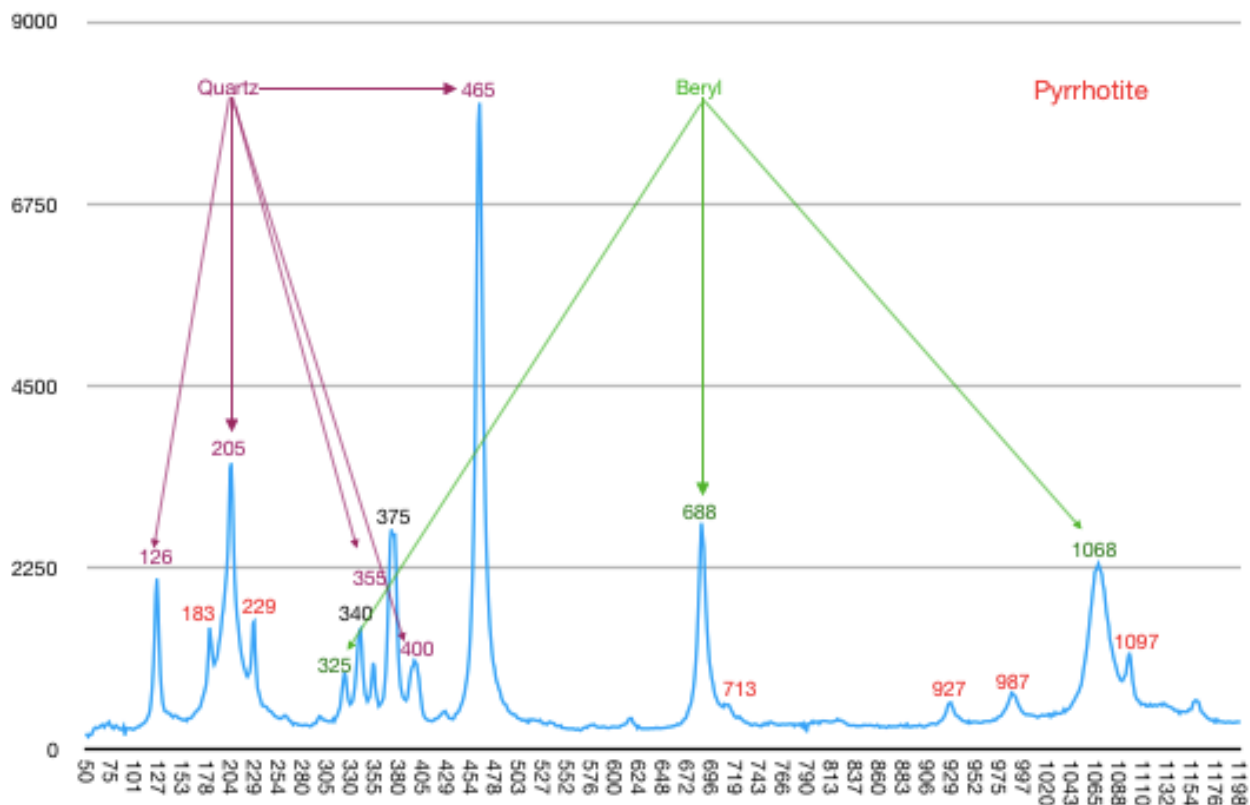
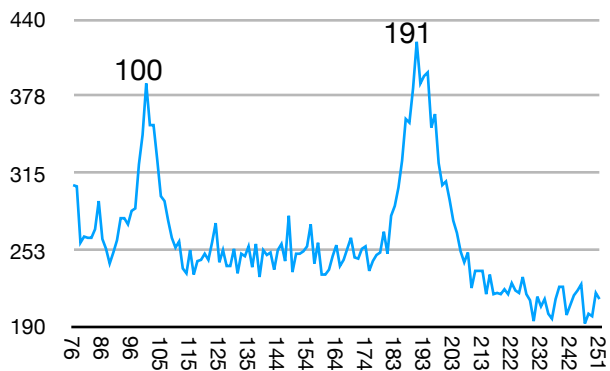
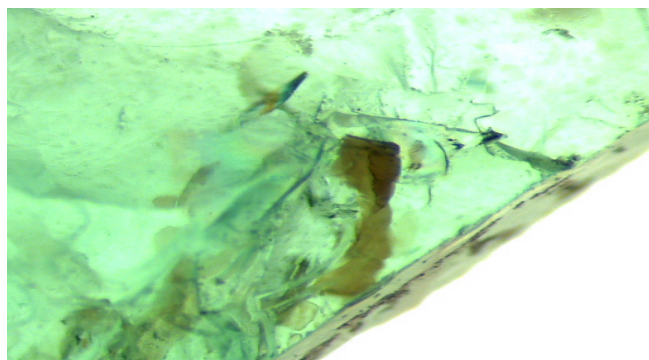


Figure 25. The black crystal in Figure 23 was determined to be Pyrrhotite by Crystal Sleuth.

JB 12 was also checked for inclusions that were near or on the surface, since it was rough. Spectrums of three inclusions were taken but only the first, of a brown anhedral inclusion, revealed any peaks other than beryl. Peaks at 100 and 191  $\text{cm}^{-1}$  revealed mica but since there were no spectral features other than the common baseline between the three scans, and in particular 300 and 400  $\text{cm}^{-1}$ , separation of biotite from phlogopite was impossible (Figures 26 and 27).



Figures 26 (Left) The inclusion, viewed at 40x. Figure 27 (Right) The inclusion in Figure 25 was an undetermined variety of mica when analyzed with microRaman spectroscopy.

#### 6.3.4 Scanning Electron Microscope with EDS

The SEM was used on several occasions for viewing and analysis of surface reaching inclusions. BR4-7 on the slide were coated with amorphous carbon and then surveyed for interesting surface reaching inclusions. BR5 and BR7 revealed interesting results.

BR5 featured an anhedral mica blob that was polished through. The Z-shaped mica inclusion was photographed at 60x in the SEM (Figure 28). Later when the carbon was removed the sample was photographed in reflected light for comparison (Figure 29).

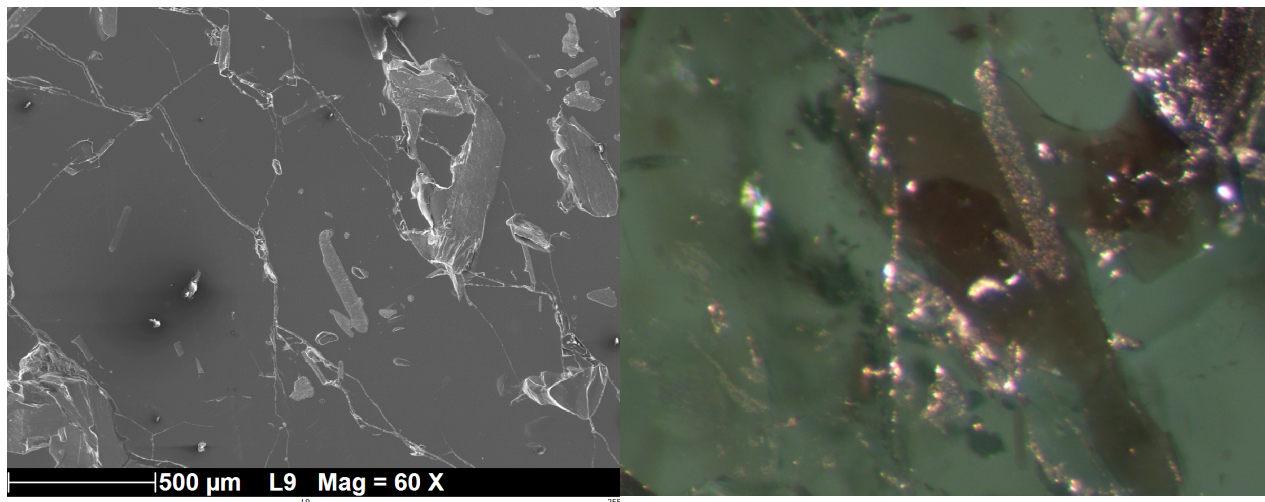
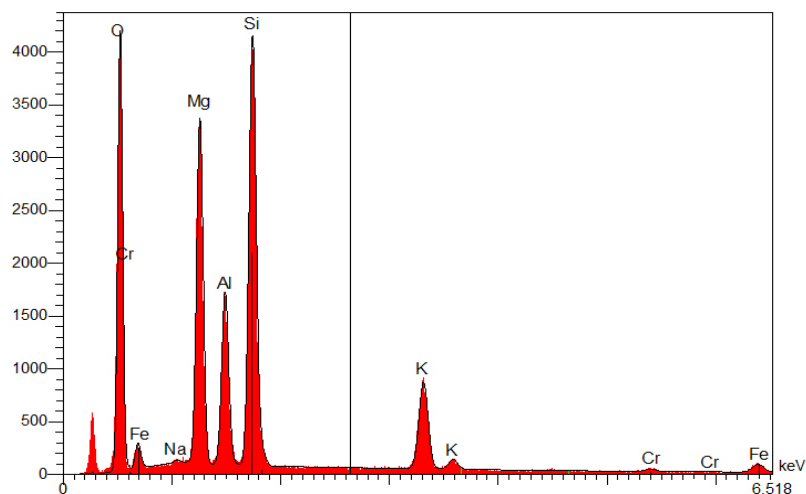


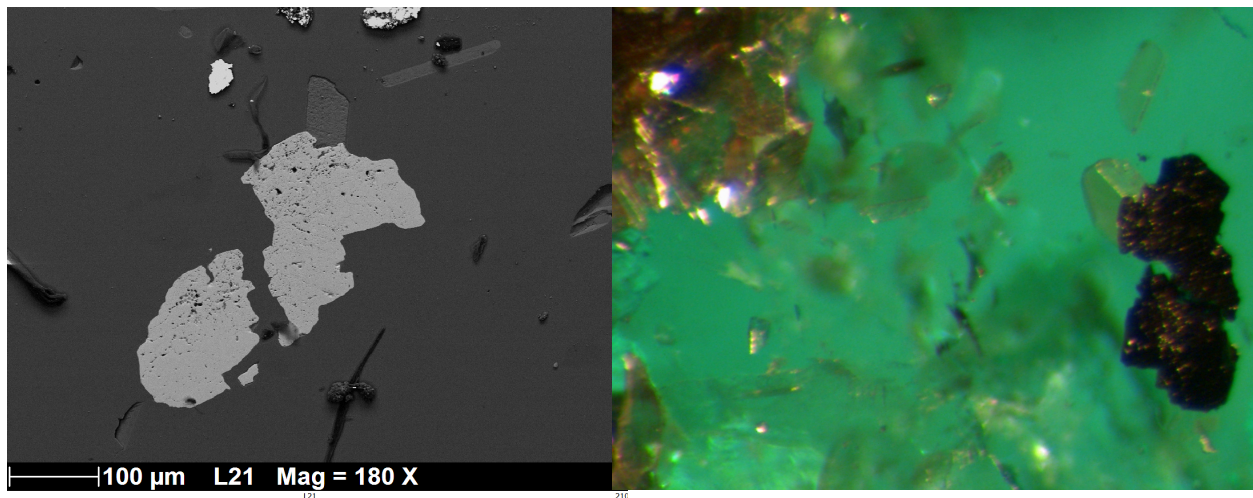
Figure 28 (Left) The mica, viewed at viewed at 60x, in the SEM was an undetermined variety of mica from the growth environment. Figure 29 (Right) shows the mica @ 70x in reflected light for comparison. Next the detector was switched to the EDS for quantitative analysis (Figure 30).



Figures 30. EDS quantitative analysis of percentage of elements elements in the mica target area.

The EDS reports percentages of elements seen within the target area, in this case, the Z-shaped inclusion. When totals are adjusted for atomic weight of elements, iron was only a small percentage of the total weight sampled. In biotite, iron is a major element of the mineral's molecular chemistry and molecular weight, at more than 16% of the total. In the case of this sample iron was a trace element at 1.22% of weight. When combined with a higher percentage of oxygen weight than we see in biotite molecules, it is possible to eliminate biotite as the variety of mica in this Ethiopian emerald. Indeed, the percentage of atoms out of 100% seen by EDS comes very close to the actual percentage of distribution of elements in phlogopite. This inclusion is phlogopite. See Appendix 3 for EDS quantitative analysis of the Z-shaped surface reaching inclusion.

BR7 also had an interesting surface reaching inclusion very close to a number of pseudo-hexagonal surface reaching mica platelets (Figure 32). The SEM views elements by atomic/molecular weight in contrast (Figure 3q), and it is possible to observe that the micas have a different density than the target inclusion.



Figures 31 (Left) The heavier inclusion, viewed at viewed at 180x, in the SEM was a mystery molecule next to lighter surface reaching micas and emerald matrix. Figure 32 (Right) shows the inclusion and mica @ 70x in transmitted light for comparison to the SEM image.

Next the detector was switched to the EDS for quantitative analysis to identify the mystery inclusion (Figure 33).

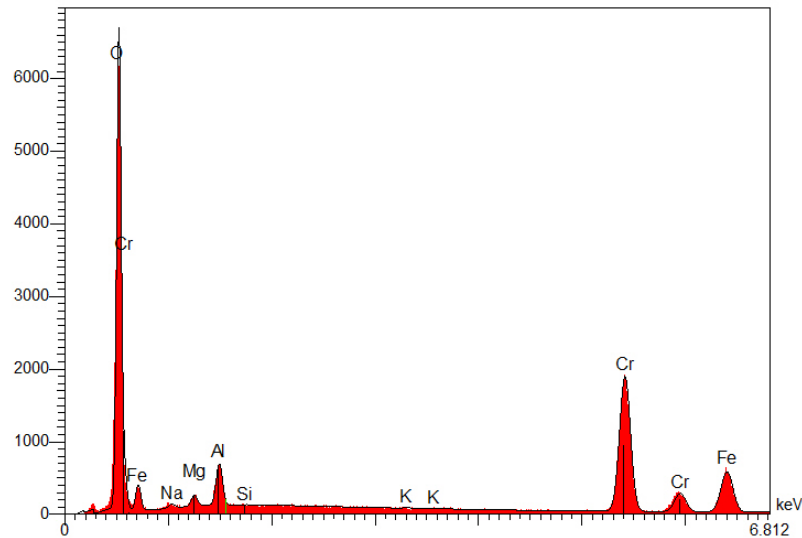


Figure 33 shows much lower numbers of magnesium, aluminum, silicon and potassium atoms than the previous inclusion identified as phlogopite. It shows much higher numbers of chromium and iron atoms.

The much higher numbers of chromium atoms and iron atoms in this quantitative analysis show that these numbers of atoms move well beyond what you might see as the coloring agents in beryl (See Appendix 4 for details). When percentage element weights of the sample are adjusted for the atomic weights of the elements sampled a molecule that is 55% oxygen atoms, 27% chromium atoms, 13% iron atoms, 3% aluminum atoms and 1% magnesium atoms is revealed. It's not an exact match in so far as the percentages of the last three elements are concerned, but the composition of a mineral with twice as many oxygen atoms as chromium atoms plus smaller amounts of iron, aluminum and magnesium is an exact match for chromite whose formula is  $(\text{Fe}, \text{Mg}, \text{Al})\text{Cr}_2\text{O}_4$ .

## 7. DISCUSSION

As a part of the formation of Gondwanaland, rare element beryllium was delivered by pegmatites into contact zones with metamorphic rocks like mica schists, and chromite-rich serpentines, in the oxidized iron-rich environment of what is now Seba Boru, Ethiopia. Through metasomatism in a mineral rich solution, these elements plus aluminum and silicon and oxygen, met and equilibrated. As this solution cooled,



mineral saturation could no longer be maintained and crystallization occurred. Only recently discovered, and hundreds of millions of years after the passing of these geological events, the emeralds of Ethiopia have arrived on the world market.

In their top grades they are exceptional for their crystal purity and lack of fractures. As such, no treatment oil or polymer can even enter the pure crystal. Marketed as “no-oil” or “no-treatment” these stones will sell for a premium in top colors and clarities because more than 90% of emerald gemstone market is oil or resin filled. In addition, the lack of fractures will mean that they are more durable than fracture-filled stones, better able to survive setting, wear and cleaning.

The picture for the Ethiopian emerald seems rosy, but there is plenty of room for confusion. Identification of these emeralds is no simple task. Emeralds from Santa Terezina (Brazil), Habachtal (Austria), Panjshir (Afghanistan), Malysheva (Russia), Swat (Pakistan), Mananjary (Madagascar) and Kafubu (Zambia), among others share a schist-based emerald genetic origin. The characteristics of emeralds from these localities may overlap Seba Boru emeralds to a very significant degree. Kafubu and Panjshir emeralds, in particular, seem to share many similarities with Seba Boru emeralds, possibly down to the way that water molecules sit in the crystal lattice and this should be studied further. The fact that Kafubu emeralds are currently 30% of the world supply means that confusion *will* have an impact on the market.

Major laboratories like GIA and SSEF have published articles indicating they can separate Ethiopian emeralds from other localities with destructive tests like LAI-CP-MS trace element chemistry. Emeralds do vary significantly, however, even in the same deposit. The chances of a 100% correct origin identification rate for these labs is slim-to-none. As evidence, in the trade important gemstones always sell with multiple certificates, proving dealers are distrustful of branded labs with big names. Stories of labs contradicting each other and even themselves *on the same stone* are more common than not.

## **CONCLUSION**

The topic of geographic origin determination is a complicated and even political subject in gemology. Like Dr. Gubelin, who invented this science of the Kashmir Sapphire and Pigeon's Blood Ruby, the auction houses that trade on it, and modern-day-Gubelin-type adventurers who make a living off of it, there is no shortage of people wanting to get a piece of the branded gemstone action. But it isn't all quite as simple as it may seem. Some famous gemologists recognize the danger in geographic origin determination and are not afraid to put it in print. Dr. Dietmar Schwarz, the noted emerald expert, wrote in 2015 in the conclusion to his In Color article on the origin determination of emerald:

“...if the geological-genetic situation is the same or nearly identical for two deposits, the emeralds from these deposits will show features that are widely overlapping. The separation of emeralds from these deposits will be extremely difficult or may not be possible at all.”

From one of the Gubelin proteges himself we hear the message loud and clear: ‘Don't believe the hype!’

## **ACKNOWLEDGEMENTS**

I would like to thank Dr. Rondeau and Prof. Fritsch for their assistance in the last few weeks finishing the research required to produce a complete research paper. Now I can say I'm satisfied with the research and associated report on one of the most exciting topics in gemology at the moment. In addition, I want to register how valuable an exercise I thought both this project and the bibliographic report were. Both projects helped me to solidify my gemological understandings of current research, gemological theory and practice. This program has been very valuable for me. Thank you.

## BIBLIOGRAPHY

Admin (1/19/14) Topkapi Dagger (Retrieved on 3/27/18). <https://www.boutiqueottoman.com/topkapi-dagger/>

Branstrator B. (3/27/17) 5 Things to Know About Ethiopian Emeralds. 10x Blog *National Jeweler*, (Retrieved on 3/6/18). <http://www.nationaljeweler.com/blog/5384-5-things-to-know-about-ethiopian-emeralds>

Cevallos P., Simmons W.B., Falster A.U. (Fall 2012). Emerald from Ethiopia. *Gem News International*, *Gems & Gemology*, 219-220.

Heebner J. (2018) Emerald Dreams. *AGTA Prism*. Vol 1, 2018, p. 8.

Krzemnicki M. S. (Feb. 2018) Ethiopia: New Source for Sapphires and Emeralds. *Facette*, Issue 24.

Lackner N. (Retrieved on 3/27/18) The Austrian Emerald Story - Without Formating Problem *GemologyOnline.com* <https://www.gemologyonline.com/Forum/phpBB2/viewtopic.php?t=307>

Laurs B. M. (Spring 2012) *Gem News International*. *Gems & Gemology*, Vol 48, No 1, pp. 66-67.

Parrot C. (July 2017) Ethiopia's Emerald Story: The Emergence of a New Treasure (Retrieved on 3/6/18) <https://www.blueniletrade.com/research/ethiopias-emerald-story/>

Pinet M., Smith D.C., Lasnier B. (June, 1992) Utilite de la Microsonde Raman pour l'Identification non-Destructive des Gemmes, *La Microsonde Raman en Gemmologie*, pp. 44-52.

Schubnel H. J. (June, 1992) Une Methode Moderne D'Identification et D'Authentification des Gemmes, *La Microsonde Raman en Gemmologie*, p. 8.

Renfro N., Sun Z., Nemeth M., Vertriest W., Raynaud V., Weeramankhonlert V. (Spring 2017) A New Discovery of Emeralds from Ethiopia. *Gems & Gemology*, Vol. 53, No. 1, pp. 114-115.

Ringsrud R. (2009) Emeralds: A Passionate Guide. pp. 284-285.

Schluessel R., Schluessel N. H. (March/April 2018). Emeralds from Ethiopia. *Gem Guide*, pp. 1-5.

Schwarz D., Pardieu V. (F/W 2009). Emeralds from the Silk Road Countries - A Comparison with Emeralds from Colombia. *InColor*, Issue 12.

Saeseaw S., Pardieu V., Sangsawong S. (Summer 2014). Three Phase Inclusions in Emerald and Their Impact on Origin Determination. *Gems & Gemology* Vol. 50, No. 2, pp. 114-132.

Sollenbruch K., Link K., Sintayehu T. (Spring 2017) Gem Quality Emeralds from Southern Ethiopia, *InColor*, Vol 12 pp. 38-43.

Streeter E.W. (1898). Precious Stones and Gems, Their History, Sources and Characteristics, Sixth Edition, London.

Vazquez Hoys A. (3/27/10) Tesoro Imperial de Topkapi (Retrieved on 3/27/18). <http://www.bloganavazquez.com/2010/03/27/tesoro-imperial-de-topkapi/>

Wainer S. (2017) Experimentals Dissertation: Pailin Fancy Color Sapphires a.k.a Tailila.

Wood D. L., Nassau K. (May-June 1968). The Characterization of Beryl and Emerald by Visible and Infrared Absorption Spectroscopy, *The American Mineralogist*, Vol. 53, pp. 777-800.

## Appendix 1

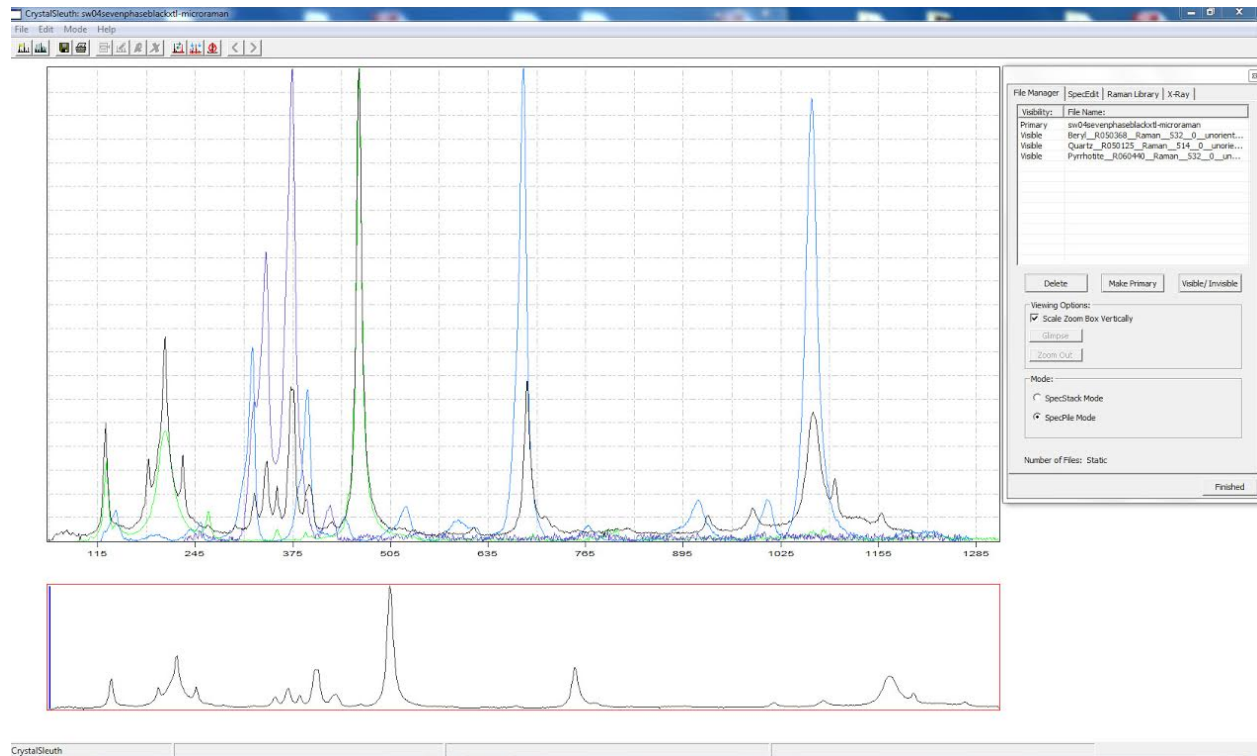
### No treatment emerald price comparison

#### Gem Guide Fall 2013 & Rapaport 2018

	<b>Emerald Extra Fine No Treat</b>	<b>Ruby Extra Fine Burma NH</b>	<b>Sapphire Extra Fine Burma NH</b>	<b>Diamond EXEXEX F,G VS</b>	<b>Diamond EXEXEX D,E VVS</b>
<b>1 Ct</b>	11,000-13,000	25,000-32,000	5,000-6,000	9,000-10,000	14,000-16,000
<b>2 Ct</b>	13,000-16,000	39,000-45,000	7,000-8,000	15,000-19,000	25,000-35,000
<b>3 Ct</b>	15,000-18,000	60,000-75,000	9,000-10,000	25,000-31,000	42,000-59,000
<b>4 Ct</b>	15,000-18,000	81,000-94,000	13,000-16,000	30,000-42,000	54,000-70,000
<b>5 Ct</b>	16,000-19,000		13,000-16,000	40,000-60,000	75,000-100,000
<b>6-8 Ct</b>	16,000-21,000		15,000-18,000		
<b>8-15 Ct</b>	20,000-27,000		18,000-25,000	61,000-90,000	116,000-145,000

## Appendix 2

### Crystal Sleuth pyrrhotite identification



## Appendix 3

### SEM EDS Quantification of Phlogopite

#### Résultats quantitatifs

Elt	Ligne	Int	Erreur	K	Kr	P%	A%	ZAF	Formule	Ox%	Pk/Bg	Class	LConf	HConf	Cat#
O	Ka	1519.0	7.2029	0.6512	0.1466	40.26	56.65	0.3705		0.00	83.33	A	39.88	40.64	0.00
Na	Ka	11.5	1.8087	0.0024	0.0007	0.14	0.13	0.5074		0.00	2.21	B	0.12	0.15	0.00
Mg	Ka	1600.0	1.8087	0.2088	0.0942	14.12	13.07	0.6685		0.00	27.18	A	13.99	14.25	0.00
Al	Ka	840.8	1.8087	0.1184	0.0493	7.65	6.38	0.6451		0.00	17.44	A	7.55	7.75	0.00
Si	Ka	2193.9	1.8087	0.7817	0.1537	21.75	17.43	0.7065		0.00	44.68	A	21.58	21.91	0.00
K	Ka	561.6	0.9404	0.1569	0.0712	8.44	4.86	0.8445		0.00	15.91	A	8.31	8.57	0.00
Cr	Ka	17.5	0.3049	0.0048	0.0048	0.58	0.25	0.8238		0.00	2.68	B	0.53	0.64	0.00
Fe	Ka	63.4	0.3049	0.0585	0.0248	3.03	1.22	0.8168		0.00	4.84	A	2.89	3.17	0.00
				1.9827	0.5452	95.97	100.00			0.00					0.00

## Appendix 4

### SEM EDS Quantification of Chromite

#### Résultats quantitatifs

Elt	Ligne	Int	Erreur	K	Kr	P%	A%	ZAF	Formule	Ox%	Pk/Bg	Class	LConf	HConf	Cat#
O	Ka	2343.0	24.2889	1.0045	0.2261	29.03	55.03	0.7762		0.00	52.08	A	28.81	29.25	0.00
Na	Ka	26.3	0.8448	0.0056	0.0016	0.53	0.70	0.2997		0.00	2.60	B	0.49	0.57	0.00
Mg	Ka	72.2	0.8448	0.0094	0.0042	0.95	1.19	0.4463		0.00	3.26	B	0.91	0.99	0.00
Al	Ka	287.8	0.8448	0.0405	0.0169	2.97	3.34	0.5678		0.00	6.32	A	2.91	3.03	0.00
Si	Ka	2.7	0.8448	0.0010	0.0002	0.03	0.03	0.6944		0.00	2.04	B	0.02	0.03	0.00
K	Ka	4.7	0.2984	0.0013	0.0006	0.06	0.05	0.9809		0.00	2.06	B	0.05	0.07	0.00
Cr	Ka	1608.4	1.3471	0.4433	0.4433	46.39	27.06	0.9545		0.00	44.23	A	45.96	46.81	0.00
Fe	Ka	522.6	1.3471	0.4828	0.2042	23.22	12.61	0.8783		0.00	18.79	A	22.85	23.59	0.00
				1.9884	0.8971	103.18	100.00			0.00					0.00